The BRCA1-Δ11q Alternative Splice Isoform Bypasses Germline Mutations and Promotes Therapeutic Resistance to PARP Inhibition and Cisplatin

Yifan Wang[1], Andrea J. Bernhardy[1], Cristina Cruz[2,3], John J. Krais[1], Joseph Nacson[1], Emmanuelle Nicolas[4], Suraj Peri[1], Hanneke van der Gulden[5], Ingrid van der Heijden[5], Shane W. O'Brien[1], Yong Zhang[6], Maribel I. Harrell[7], Shawn F. Johnson[8], Francisco J. Candido Dos Reis[9,10], Paul D. P. Pharoah[10], Beth Karlan[11], Charlie Gourley[12], Diether Lambrechts[13], Georgia Chenevix-Trench[14], Håkan Olsson[15], Javier J. Benitez[16], Mark H. Greene[17], Martin Gore[18], Robert Nussbaum[19], Siegal Sadetzki[20], Simon A. Gayther[21], Susanne K. Kjaer[22], kConFab Investigators[23], Alan D. D'Andrea[24,25], Geoffrey I. Shapiro[8,26], David L. Wiest[6], Denise C. Connolly[1], Mary B. Daly[27], Elizabeth M. Swisher[7], Peter Bouwman[5], Jos Jonkers[5], Judith Balmaña[2], Violeta Serra[3], and Neil Johnson[1,*]

1. *[1]Molecular Therapeutics Program, Fox Chase Cancer Center, Philadelphia, Pennsylvania.*
2. *[2]High Risk and Cancer Prevention Group, Vall d'Hebron Institute of Oncology, Barcelona, Spain.*
3. *[3]Experimental Therapeutics Group, Vall d'Hebron Institute of Oncology, Barcelona, Spain.*
4. *[4]Cancer Biology Program, Fox Chase Cancer Center, Philadelphia, Pennsylvania.*
5. *[5]Division of Pathology, The Netherlands Cancer Institute, Amsterdam, the Netherlands.*
6. *[6]Immune Cell Development and Host Defense Program, Fox Chase Cancer Center, Philadelphia, Pennsylvania.*
7. *[7]Department of Obstetrics and Gynecology and Medicine, University of Washington, Seattle, Washington.*
8. *[8]Department of Medical Oncology, Dana-Farber Cancer Institute and Harvard Medical School, Boston, Massachusetts.*
9. *[9]Department of Gynecology and Obstetrics, Ribeirao Preto Medical School, University of Sao Paulo, Sao Paulo, Brazil.*
10. *[10]Centre for Cancer Genetic Epidemiology, University of Cambridge, Cambridge, United Kingdom.*
11. *[11]Women's Cancer Program at the Samuel Oschin Comprehensive Cancer Institute, Cedars-Sinai Medical Center, Los Angeles, California.*
12. *[12]University of Edinburgh Cancer Research UK Centre, MRC IGMM, Edinburgh, United Kingdom.*
13. *[13]VIB Vesalius Research Center, University of Leuven, Leuven, Belgium.*
14. *[14]QIMR Berghofer Medical Research Institute, Herston, Australia.*
15. *[15]Departments of Cancer Epidemiology and Oncology, Lund University, Lund, Sweden.*
16. *[16]Human Genetics Group and Human Genotyping Unit Spanish National Cancer Research Centre (CNIO), Madrid, Spain.*
17. *[17]Division of Cancer Epidemiology and Genetics, National Cancer Institute, Rockville, Maryland.*
18. *[18]Royal Marsden NHS Foundation Trust, London, United Kingdom.*
19. *[19]University of California San Francisco, Cancer Risk Program, San Francisco, California.*
20. *[20]Gertner Institute for Epidemiology and Health Policy Research, Sheba Medical Center, Tel Hashomer, Israel.*
21. *[21]Department of Preventive Medicine, Keck School of Medicine, University of Southern California Norris Comprehensive Cancer Center, Los Angeles, California.*
22. *[22]Department of Virus, Lifestyle and Genes, Danish Cancer Society Research Center, Copenhagen, Denmark.*
23. *[23]University of Melbourne, Melbourne, Australia.*
24. *[24]Department of Radiation Oncology, Dana-Farber Cancer Institute and Harvard Medical School, Boston, Massachusetts.*
25. *[25]Department of Pediatrics, Children's Hospital and Harvard Medical School, Boston, Massachusetts.*
26. *[26]Department of Medicine, Brigham and Women's Hospital and Harvard Medical School, Boston, Massachusetts.*
27. *[27]Risk Assessment Program, Fox Chase Cancer Center, Philadelphia, Pennsylvania.*

*Corresponding Author:
Neil Johnson, Molecular Therapeutics Program, Fox Chase Cancer Center, Philadelphia, PA 19111.
Phone: 215-728-7016; Fax: 215-728-2741; E-mail: neil.johnson@fccc.edu

Abstract

Breast and ovarian cancer patients harboring *BRCA1/2* germline mutations have clinically benefitted from therapy with PARP inhibitor (PARPi) or platinum compounds, but acquired resistance limits clinical impact. In this study, we investigated the impact of mutations on *BRCA1* isoform expression and therapeutic response. Cancer cell lines and tumors harboring mutations in exon 11 of *BRCA1* express a *BRCA1-Δ11q* splice variant lacking the majority of exon 11. The introduction of frameshift mutations to exon 11 resulted in nonsense-mediated mRNA decay of full-length, but not the *BRCA1-Δ11q* isoform. CRISPR/Cas9 gene editing as well as overexpression experiments revealed that the BRCA1-Δ11q protein was capable of promoting partial PARPi and cisplatin resistance relative to full-length BRCA1, both *in vitro* and *in vivo*. Furthermore, spliceosome inhibitors reduced BRCA1-Δ11q levels and sensitized cells carrying exon 11 mutations to PARPi treatment. Taken together, our results provided evidence that cancer cells employ a strategy to remove deleterious germline *BRCA1* mutations through alternative mRNA splicing, giving rise to isoforms that retain residual activity and contribute to therapeutic resistance.

Introduction

Germline mutations in the *BRCA1* gene are associated with an increased risk of developing breast and ovarian cancer (1, 2). Mutations often result in reading frameshifts and nonsense-mediated mRNA decay (NMD; ref. 3). The BRCA1 protein is essential for efficient homologous recombination (HR)-mediated repair of double-stranded DNA breaks (4, 5). Inhibitors of PARP, as well as platinum agents, induce double-stranded DNA breaks that are repaired by the HR DNA repair pathway (6, 7). Consequently, cells that have defective HR DNA repair, such as those with dysfunctional BRCA1 or BRCA2 proteins, are highly sensitive to PARP inhibitor (PARPi) or platinum treatments (8–11).

Although PARP inhibitors have been shown to provide survival improvements, many patients that harbor germline *BRCA1* or *BRCA2* mutations do not gain benefit from PARPi therapy (12–14). In addition, many patients that first benefit from either PARPi or platinum therapy develop disease progression and resistance (15). PARPi or platinum resistance has been demonstrated to arise by a variety of mechanisms, including reversion mutations (16, 17), loss of 53BP1 pathway activity (18, 19), expression of hypomorphic BRCA1 proteins (20, 21), and drug efflux (22).

BRCA1 mRNA isoforms generated by alternative splicing lack specific exons and have been shown to be expressed in cells and tissues (23–25). In particular, the relative levels of *BRCA1* exon 11 splice isoforms differ between normal and cancer tissues and in discrete phases of the cell cycle (26–29). These isoforms include *BRCA1* full-length (inclusion of all coding exons), Δ11 (skipping of exon 11), and Δ11q (partial skipping of exon 11). The *BRCA1-Δ11q* isoform derives from use of an alternative exon 11 splice donor site, resulting in the exclusion of most exon 11 nucleotides (c.788-4096; Supplementary Fig. S1; refs. 27, 28). In human cells and tissues, the *BRCA1-Δ11q* isoform expression is more readily detectable than the *BRCA1-Δ11* isoform (26, 29, 30).

The BRCA1-Δ11 isoform has previously been implicated in both cell death and proliferation in mouse studies. Both *Brca1*-null and $Brca1^{\Delta 11/\Delta 11}$ mice that exclusively express Brca1-Δ11 undergo embryonic lethality, but $Brca1^{\Delta 11/\Delta 11}$ embryos die at a later stage, suggesting that Brca1-Δ11 isoform can partially compensate for the lack of other Brca1 isoforms during embryogenesis (31–33). *BRCA1* mutations located in exon 11 represent approximately 30% of the overall number of mutation carriers that develop breast and ovarian cancer in the United States (34–37). Here, we examined the impact of exon 11 mutations on *BRCA1* isoform expression and therapy response.

Materials and Methods

Cell lines and reagents

Cells were purchased from Asterand or ATCC. Cycloheximide (CHX), actinomycin D (ACT), puromycin, blasticidin, and DMSO were purchased from Sigma-Aldrich, cisplatin was from APP/Fresenius Kabai USA LLC, and paclitaxel from Sagent Pharmaceuticals. Pladienolide B (Pl-B) was purchased from Calbiochem. Clovis Oncology provided rucaparib (CO-338) and olaparib (AZD2281) was purchased from Selleckchem. *BRCA1*-mutated cell lines were validated through DNA sequencing and the identification of specific *BRCA1* mutations that are uniquely present in individual cell lines as well as DNA fingerprinting. Cell lines tested negative for mycoplasma.

Colony formation assays

Depending on colony-forming potential, cells were seeded at a density ranging from 500 to 4,000 cells per well in 6-well plates in the presence of increasing concentrations of either rucaparib or olaparib. For cisplatin and taxol treatments, exponentially growing cells were cultured in 24-well plates, treated with increasing concentrations of cisplatin and taxol for 24 hours, and replated in 6-well plates for colony formation. For shRNA or cDNA add back colony formation experiments, cells were treated as above, but with the addition of either puromycin or blastcitidin in the media. For siRNA treatments, exponentially growing cells were reverse transfected in 24-well plates, and 2 days after transfection, cells were treated with rucaparib for 72 hours and then replated in 6-well plates for colony formation. For Pl-B colony assays, cells were treated with Pl-B (1.25 nmol/L) and rucaparib (100 nmol/L) for 72 hours and then replated into 6-well plates for colony formation. Colony formation was assessed 2 weeks postplating with crystal violet staining. Mean colony formation from three experiments was expressed as percentage of colonies $\pm$ SE relative to vehicle-treated cells.

Gene sequencing and RT-PCR analysis

Genomic DNA was isolated from cells using the DNeasy tissue kit (Qiagen). To determine whether gene rearrangements had taken place that would have excluded the exon 11q region from genomic DNA of cell lines and patient-derived xenograft (PDX) tumors, we carried out PCR using OneTaq Hot Start 2X Master Mix (NEB) and gDNA as templates. Primers were located in exon 10 (forward, F) and 12 (reverse, R): F:aatcacccctcaaggaacca; R:ctcacacccagatgctgcttc. Total RNA was isolated from cell lines using RNeasy Kit (Qiagen). For quantitative RT-PCR, RNA was tested for quality on a Bioanalyzer (Agilent). RNA concentrations were determined with a spectrophotometer (NanoDrop; Thermo Fisher Scientific). RNA was reverse transcribed using Moloney murine leukemia virus reverse transcriptase (Ambion) and a mixture of anchored oligo-dT and random decamers. Two reverse transcription reactions were performed for each sample using either 100 or 25 ng of input RNA. Assays were used in combination with TaqMan Universal Master mix or Power SybrGreen Master Mix and run on a 7900 HT sequence detection system (Applied Biosystems). Cycling conditions were 95°C, 15 minutes, followed by 40 (two-step) cycles (95°C, 15 seconds; 60°C, 60 seconds). C_t (cycle threshold) values were converted to quantities (in arbitrary units) using a standard curve (four points, 4-fold dilutions) established with a calibrator sample. For each sample, the values were averaged and SD of data derived from two independent PCRs. For the *BRCA1* splice variants, amplicons quantified by on-chip electrophoresis on an Agilent 2100 Bioanalyzer were used for absolute quantification assays. Primers that specifically recognize the following *BRCA1* mRNA isoforms were used: exon +11 containing: F:tagcaaggagccaacataacagat; R:cttattccattcttttctctcacacag; Δ11q: F:gattctgcaaaaaaggctgct; R:cagatgctgcttcaccctga.
For *RBFOX2* F:aagcccagtagttggagctgt, R:ttgcctagggacacatctgctt; and *POLR2F*: F:tgccatgaaggaactcaagg R: tcatagctcccatctggcag. BRCA1 expression values were routinely normalized to a *POL2RF* housekeeping gene (HKG) control and expressed as a percentage of the values calculated for MDA-MB-231 cells or to a relevant control sample.

BRCA1-minigene generation and analysis

Genomic DNA derived from blood lymphocytes of healthy individuals was tested for the absence of mutations by BROCA sequencing. The entire genomic region of *BRCA1* from exon 8 to exon 12 was amplified with the following 5 PCR reactions and primer sets:

- 1F: ccgctcgagAACCTTGGAACTGTGAGAACTCTG
- 1R: ccggatatCAATTTGAGAGCCCAGTTTGAAT
- 2F: ccgctcgagAACCTGGGTGACAGAGCAAGA
- 2R: ccggatatcAGGGAAAAGACAGAGTCCTAATAAGA
- 3F: ccgctcgagAGAGCTAAAATGTTTGATCTTGGTC
- 3R: ccggatatcTCTTGATAAAATCCTCAGGATGAAG
- 4F: ccgctcgagATTTGGGAAAACCTATCGGAAG
- 4R: ccggatatcTAATACTGGAGCCCACTTCATTAGT
- 5F: ccgctcgagCCAGCTCAAGCAATATTAATGAAGT
- 5R: ccggatatcGTTAAAATGTCACTCTGAGAGGATAGC

HA-tag was cloned into pENTRA vector using *Sal*I and *Xho*I sites. Each *BRCA1* fragment was first cloned into pENTRA-HA vector using *Xho*I (shown in lowercase forward primers above) and *Eco*RV (shown in lowercase reverse primers above) sites. The 5 cloned fragments were assembled into a minigene using the following restriction sites that corresponded with cut sites in each fragment: *Eco*RI, *Spe*I, *Stu*I, and *Sca*I sites. An eGFP fragment was cloned into the 3′end of the exon 12 fragment using *Eco*RV site. The minigene was then shuttled into pcDNA6.2 Destination vector using the LR Clonase system (Invitrogen). We confirmed by Sanger sequencing that mutations were not introduced into exons or introns within 500 bp flanking each exon. The indicated mutations (see Supplementary Fig. S3A) were introduced using site-directed mutagenesis (Agilent) using the following primers:

- 2288delT F: ccagtgaacttaaagaatttgtcaacctagccttccaaga
- 2288delT R: tcttggaaggctaggttgacaaattctttaagttcactgg
- 2529C>T F: caaatgctgcacactaactcacacatttatttggttctgtttttg
- 2529C>T R: caaaaacagaaccaaataaatgtgtgagttagtgtgcagcatttg
- 3960C>T F: ctaaggtgatgttcctaagatgcctttgccaatattacc
- 3960C>T R: ggtaatattggcaaaggcatcttaggaacatcaccttag
- 1stFOXMut F: tcagggtagttctgtttcaaacttacacgtggagccatgtg

- 1stFOXMut R: cacatggctccacgtgtaagtttgaaacagaactaccctga
- 2ndFOXMut F:gagtaataaactgctgttctcgtgttgtaatgagctggcatgagta
- 2ndFOXMut R: tactcatgccagctcattacaacacgagaacagcagtttattactc
- Ex11qsplice F: tgcaagtttgaaacagaactcccctgatacttttctggatg
- Ex11qsplice R: catccagaaaagtatcaggggagttctgtttcaaacttgca

To measure *BRCA1-Δ11q*-reporter expression, total RNA was isolated from transfected cells using RNeasy Kit (Qiagen). cDNA was synthesized using High-Capacity cDNA Reverse Transcription Kit (Applied Biosystems). PCR was performed using OneTaq Hot Start 2X Master Mix (NEB). Primers that specifically recognize *BRCA1-Δ11q*-reporter mRNA were: F: gattctgcaaaaaaggctgct; R: agtcgtgctgcttcatgtggt; and *BSD*: F: gcctttgtctcaagaagaatcca; R: tagccctcccacacataacca. In addition, Western blots using HA antibody detected BRCA1-Δ11q-reporter protein expression.

Western blotting

Western blotting was carried out as described previously and proteins detected using the following antibodies: BRCA1: N-terminal: (MS110, EMD), C-terminal: (D9, Santa Cruz Biotechnology), BRCA1 (9010, Cell Signaling Technology), tubulin (2148, Cell Signaling Technology), HA (23675, Cell Signaling Technology), RAD51 (H-92, Santa Cruz Biotechnology), Pol II [C-18, (Santa Cruz Biotechnology)], CtIP (A300-438-A, Bethyl Laboratories), PALB2 (A301-247A1, Bethyl Laboratories), BARD1 (A300-263A, Bethyl Laboratories), and BRCA2 (OP-95, EMD). HA (23675, Cell Signaling Technology) antibody was used for immunoprecipitation of HA-BRCA1 complexes from 2 mg of nuclear extract using Pierce Classic IP Kit (Thermo Scientific) according to the manufacturer's instructions. Nuclear extracts were derived using NE-PER Nuclear and Cytoplasmic Extraction Reagents (Thermo Scientific) according to the manufacturer's instructions. Densitometric analyses were carried out using ImageJ software.

Immunofluorescence and microscopy

For immunofluorescence HA (HA.11, Covance), BRCA1 (MS110, EMD), γ-H2AX (pS139; N1-4131, EMD) and RAD51 (H-92, Santa Cruz Biotechnology), geminin (10802-1-AP, ProteinTech Group) and geminin (Abnova, E7071-1A8) antibodies were followed by secondary antibodies conjugated to FITC or Texas Red (Jackson ImmunoResearch Laboratories). We acquired immunofluorescence images using Nikon NIU Upright Fluorescent Microscope and generated images using Nikon NIS Elements software. For IR experiments, we routinely fixed cells 8 hours after treatment with 10 Gy. For analyses, we counted a minimum of 200 cells per condition or cell line. Foci-positive cells were expressed as a percentage of geminin-positive cells to account for any differences in S–G_2–M populations between cell lines. Each experiment was carried out three times with biologic replicates. γ-H2AX IRIF was present equally in all cell lines and routinely measured as a positive control for IRIF.

Immunofluorescence and immunohistochemical analyses of tumors

For BRCA1 focus formation analysis, tissue sections were deparaffinized with xylene and hydrated with decreasing concentrations of ethanol. For target antigen retrieval, sections were microwaved in Dako Antigen Retrieval Buffer pH 9.0 for 4 minutes at 110°C [a T/T MEGA multifunctional Microwave Histoprocessor (Milestone)]. Sections were cooled down in distilled water for 5 minutes, and then permeabilized with Dako Wash Buffer containing Tween 20 for 5

minutes, followed by incubation in blocking buffer (Dako Wash Buffer with 1% BSA) for 5 minutes. Primary antibodies were diluted in Dako Antibody Diluent and incubated at room temperature for 1 hour [anti-BRCA1 Abcam MS110 diluted 1:200; anti-Geminin (ProteinTech Group, 10802-1-AP, diluted 1:400)]. Sections were washed for 5 minutes in Dako Wash Buffer followed by 5 minutes in blocking buffer. Secondary antibodies (Alexa Fluor 488 or 568) were diluted 1:500 in blocking buffer and incubated for 30 minutes at room temperature. The two-step washing was repeated followed by 5 minutes incubation in distilled water. Dehydration was performed with increasing concentrations of ethanol. Sections were mounted with DAPI ProLong Gold antifade reagent and stored at −20°C. For analyses, tumors from 2 mice per treatment group were analyzed and counted. For each tumor, a minimum of 100 geminin-positive cells were identified and counted for those that had at least 5 BRCA1 foci. BRCA1 foci–positive cells were calculated as a percentage of geminin-positive cells.

For assessment of Ki-67 and γ-H2AX by IHC, slides were deparaffinized and hydrated. Antigen retrieval was performed using pH 9 EDTA buffer (DAKO, S2368). Endogenous peroxidases were quenched by immersion of slides in 3% hydrogen peroxide solution (30% H_2O_2, Fisher BP2633-500, diluted in methanol). Primary antibody Ki-67 (Clone EP5), Epitomics, (1:1,500), or γ-H2AX (pS139; N1-4131, EMD; 1,20,000) were diluted with DaVinci Green Diluant (Biocare Medical, PD900) and incubated on slides overnight at 4 degrees in a humidified slide chamber. Slides were then washed 3 times in TBST and incubated with Envision+ System HRP Labelled Polymer Anti-Rabbit (Dako, K4003) for 1 hour at room temperature. Specimens were washed 3 times in TBST and then developed with DAB solution (Dako, K3468) and counterstained in Meyer Hematoxylin (Dako, S3309). For analyses of Ki67 and γ-H2AX expression, a minimum of 2 tumors derived from 2 separate mice were used. Mice were treated with rucaparib 150 mg/kg two times per day for 4 continuous days. For cisplatin, mice were treated with a single dose of 6 mg/kg. Tumors were resected and formalin fixed 4 days from the first dose. A minimum of 2 tumors and 3 images per tumor were used to calculate staining intensities. Image staining intensities were measured using ImageJ analysis software.

PDX tumor derivation, xenograft treatments, and analyses

For PDXs, patient consent for tumor use in animals was completed under a protocol approved by the Vall d'Hebron Hospital Clinical Investigation Ethical Committee and Animal Use Committee. Mice were maintained and treated in accordance with institutional guidelines of Vall d'Hebron University Hospital Care and Use Committee. Tumors were subcutaneously implanted in 6-week-old female HsdCpb:NMRI-*Foxn1*^{nu} mice (Harlan Laboratories). Animals were supplemented with 1 μmol/L estradiol (Sigma) in the drinking water. Upon xenograft growth, tumor tissue was reimplanted into recipient mice, which were randomized upon implant growth. Mice were allocated in control/treated groups to deliver similar mean and SE when tumor volume reached between 150 and 300 mm^3 without any blinding. Vehicle or olaparib was administered at 50 mg/kg per oral gavage 6 days per week. Tumor xenografts were measured with calipers and tumor volumes were determined using the formula: (length × $width^2$). At the end of the experiment, animals were killed by CO_2 inhalation. Tumor volumes are plotted as mean ± SEM. Relative tumor volume RTV for vehicle-treated mice and individual RTVs are shown for olaparib-treated mice. For xenograft studies, MDA-MB-436 cells were subcutaneously implanted in 6-week-old female NSG mice (NOD.Cg-*Prkdc*^{scid} *Il2rg*^{tm1Wjl}/SzJ). When tumors reached approximately 300 mm^3, tumors were harvested and cut up into smaller pieces followed by subcutaneous reimplantation. Treatment was initiated when tumors reached between 150 and 180 mm^3. Rucaparib was administered at 150 mg/kg twice daily for 10 continuous days with a 2-day break after the first 5 days. Cisplatin was administered at a single dose of 6 mg/kg. Tumors were measured with calipers and tumor volumes calculated as described above. Measurements were carried out every 2 days and mice were euthanized when tumors reached 1,500 mm^3 in accordance with institutional guidelines of Fox Chase Cancer Center (Philadelphia, PA).

Statistical analyses

Mean and SE values were compared using unpaired *t* tests (GraphPad Software). $P < 0.05$ was considered statistically significant. Asterisks indicate statistically significant *P* values. There were similar variances between statistical groups compared. All statistical tests were unpaired *t* tests unless otherwise stated next to the *P* value.

Results

Cell lines with exon 11 mutations express BRCA1-Δ11q

To examine the impact of *BRCA1* exon 11 mutations on the expression of BRCA1 proteins, we employed a panel of human cancer cell lines that were either *BRCA1* wild-type or harbored known deleterious *BRCA1* mutations (Supplementary Fig. S2A). Full-length BRCA1 protein was detectable in MDA-MB-231, MCF7, and MDA-MB-468 wild-type *BRCA1* cell lines, but was absent in all *BRCA1* mutation–containing cell lines. A band corresponding with the predicted molecular weight (~89 kDa) of the BRCA1-Δ11q isoform was present in *BRCA1* wild-type cell lines, as well as L56Br-C1, SUM149PT, and UWB1.289 cell lines that harbored *BRCA1* exon 11 frameshift mutations (**Fig. 1A**).

To establish the identity of the isoform detected below the 100-kDa mark, we transfected cells with a siRNA designed to specifically target BRCA1-Δ11q and measured protein expression. BRCA1-Δ11q siRNA did not impact the levels of the full-length, but dramatically reduced the expression of the predicted BRCA1-Δ11q isoform (**Fig. 1B**). Furthermore, we confirmed that cells did not harbor secondary *BRCA1* reversion mutations or genomic rearrangements (Supplementary Fig. S2).

Next, we investigated the levels of *BRCA1* mRNA containing exon 11 (+11) as well as the *BRCA1-Δ11q* (Δ11q) isoform expression. L56Br-C1, SUM149PT, and UWB1.289 exon 11–mutant cell lines exhibited 3- ($P < 0.001$), 3- ($P < 0.001$), and 2.9-fold ($P < 0.001$) lower expression of +11 transcripts, respectively, relative to MDA-MB-231 cells (**Fig. 1C**). In contrast, relative Δ11q expression was 1.46- ($P = 0.0148$), 1.55- ($P < 0.001$), and 1.58-fold ($P = 0.0136$) higher in L56Br-C1, SUM149PT, and UWB1.289, respectively, relative to MDA-MB-231 cells expression levels (**Fig. 1C**).

Robust *BRCA1* gene transcription promotes BRCA1-Δ11q expression

To investigate the impact of germline mutations on exon 11 splicing, we introduced a series of exon 11 frameshift mutations into a *BRCA1*-minigene system (Supplementary Fig. S3). Mutation of the exon 11q splice junction disrupted Δ11q-reporter mRNA and protein expression. However, three different frameshift mutations at various locations throughout exon 11 had no effect on Δ11q-reporter expression (**Fig. 1D**). Moreover, RNA-seq analyses of mRNA splice junctions did not indicate that higher levels of *BRCA1-Δ11q* expression in cell lines with exon 11 mutations were due to increased global alterations in splicing (Supplementary Table S1).

To further investigate the effects of exon 11 mutations on *BRCA1-Δ11q* levels, we used CRISPR/Cas9 technology to generate SUM149PT cells that either had additional out of frame mutations, or reversion mutations that restored the reading frame (Supplementary Fig. S4). In line with minigene data, the introduction of additional out-of-frame or frame-restoring mutations in exon 11 did not affect *BRCA1-Δ11q* expression (**Fig. 1E**). However, clones 3 and 4 that had restored *BRCA1* reading frames, expressing the BRCA1-long-form protein product, had 2.5- ($P < 0.0001$) and 2.47-fold ($P < 0.0001$) increased levels of +11 expression, respectively, relative to sg_GFP control cells (**Fig. 1E**), likely resulting from premature translation termination codon (PTC) removal, enabling +11 containing transcripts to avoid NMD (**3**).

We confirmed that NMD contributed to the low levels of +11 mRNA detected in exon 11 mutation containing cell lines by treating cells with CHX, an inhibitor of NMD (**Fig. 1F**; ref. **38**). CHX

treatment for 5 hours resulted in a 2.8- (P = 0.0007), 3.2- (P = 0.023), and 2.9-fold (P = 0.0024) increase in +11 levels in L56Br-C1, SUM149PT, and UWB1.289 exon 11–mutant cell lines, respectively, but did not affect +11 levels in wild-type MDA-MB-231 cells, or Δ11q mRNA levels in any of the cell lines (Fig. 1F).

The increase in +11 mRNA resulting from inhibition of NMD led us to predict that exon 11–mutant cell lines have robust *BRCA1* gene transcription. To test this possibility, we treated cells with the transcription inhibitor ACT and measured *BRCA1* mRNA levels. MDA-MB-231 cells treated with ACT had a 1.4-fold (P = 0.0002) reduction in +11 mRNA levels compared with vehicle-treated cells. However, ACT treatment reduced +11 levels 3-fold (P = 0.0133) in SUM149PT cells compared with vehicle-treated cells, and completely abrogated the CHX-mediated increase in +11 mRNA (Fig. 1G). ACT also reduced Δ11q levels 1.6-fold (P = 0.002) and 2-fold (P = 0.021) in MDA-MB-231 and SUM149PT cells, respectively, compared with vehicle treatments (Fig. 1H).

Exon 11–mutant cells demonstrate partial PARPi and cisplatin resistance

We next measured the ability of exon 11–mutant cells to form BRCA1 and RAD51 foci. *BRCA1* wild-type as well as exon 11–mutant cell lines formed robust BRCA1 and RAD51 γ-irradiation–induced foci (IRIF). In contrast, BRCA1 and RAD51 IRIF were low or undetectable in cells that harbored *BRCA1* mutations outside of exon 11 (Fig. 2A).

SUM1315MO2, HCC1395, and MDA-MB-436 cell lines were highly sensitive to treatment with the PARPis rucaparib and olaparib. In contrast, exon 11 mutation containing L56Br-C1, SUM149PT, and UWB1.289 cells displayed intermediate PARPi sensitivity. SUM1315MO2, HCC1395, and MDA-MB-436 cell lines were also more sensitive to cisplatin treatment compared with L56Br-C1, SUM149PT, and UWB1.289 cells. The presence of *BRCA1* exon 11 mutations did not impact taxol sensitivity (Fig. 2B; Supplementary Table S2).

In cell growth experiments, *BRCA1* wild-type cells continuously cultured in the presence of PARPi or cisplatin proliferated at the same rate as vehicle-treated cells (Fig. 2C). Exon 11–mutant cell lines proliferated at a reduced rate in the presence of PARPi or cisplatin (Fig. 2C). MDA-MB-436 and HCC1395 cell lines harbor BRCT domain mutations and lost viability in the presence of PARPi or cisplatin. PARPi and cisplatin initially had a greater impact on the proliferation rate of UWB1.289 cells, but over time proliferation gradually increased, and corresponded with increased expression of BRCA1-Δ11q (Fig. 2D). Importantly, depletion of the BRCA1-Δ11q using 2 BRCA1 shRNAs reduced RAD51 IRIF 6.8- (P = 0.0021) and 5.7-fold (P = 0.0027) in SUM149PT, as well as 6- (P = 0.0014) and 4.7-fold (P = 0.0016) in UWB1.289 cells, compared with nontarget (NT) shRNA cells (Fig. 2E). Furthermore, BRCA1 shRNA sensitized SUM149PT and UWB1.289 cells to both PARPi and cisplatin treatments (Fig. 2F; Supplementary Table S2).

BRCA1-Δ11q is functional but inferior to BRCA1 full-length

To more finely assess the ability of BRCA1-Δ11q to provide resistance to therapy, we used CRISPR/Cas9–mediated gene editing to modify *BRCA1* in SUM149PT cells (Supplementary Fig. S4). SUM149PT cells were subject to an sg_GFP control, or sg_exon11 targeting the mutation-containing region of exon 11. Mutations introduced by sg_exon11 were either out of frame (out-frame) or restored the *BRCA1* reading frame (in-frame). Moreover, cell lines that expressed sg_exon22 demonstrated frameshift mutations in exons 22, resulting in loss of BRCA1-Δ11q expression (Fig. 3A and Supplementary Fig. S4). BRCA1-Δ11q expression in sg_exon11–treated clones with unrestored reading frames was identical to sg_GFP control cells and there were no differences in PARPi and cisplatin sensitivity in colony formation assays. However, sg_exon11 in-frame clone 3 was 226- (P = 0.0174) and 3.7-fold (P = 0.0009) more resistant to PARPi and cisplatin, respectively, and clone 4 was 207- (P < 0.0001) and 3.6-fold (P = 0.0058) more resistant to PARPi and cisplatin, respectively, compared with sg_GFP cells. In contrast,

sg_exon22 cells were 31.4- (P = 0.0183) and 2.3-fold (P = 0.0059) more sensitive to PARPi and cisplatin, respectively, compared with sg_GFP cells (Fig. 3B).

We also compared the ability of ectopic BRCA1 full-length and BRCA1-Δ11q to rescue PARPi and cisplatin sensitivity (Fig. 3C). MDA-MB-436 cells harbor a *BRCA1*$^{5396+1G>A}$ mutation that results in protein misfolding, undetectable BRCA1 protein and RAD51 IRIF, as well as exquisite PARPi and cisplatin sensitivity (20, 39, 40). MDA-MB-436 cells expressing BRCA1 full-length demonstrated robust rescue and were 179- (P = 0.0063) and 4.6-fold (P = 0.0002) more resistant to PARPi and cisplatin, respectively, compared with mCherry control cells. BRCA1-Δ11q was less effective at rescue, and cells were 19- (P = 0.0493) and 2.8-fold (P = 0.0004) more resistant to PARPi and cisplatin, respectively, compared with mCherry control cells (Fig. 3D). Moreover, when we introduced an L304P mutation (equivalent to L1407P in full-length BRCA1) that blocks the BRCA1-PALB2 interaction (41), BRCA1-Δ11q–mediated PARPi and cisplatin rescue was abolished (Fig. 3D).

Both BRCA1 full-length and BRCA1-Δ11q–expressing cells formed BRCA1 and RAD51 IRIF. However, BRCA1-Δ11q expressing cells exhibited 1.9- (P = 0.0053) and 1.9-fold (P = 0.0141) lower levels of BRCA1 and RAD51 IRIF, respectively, than full-length BRCA1-expressing cells, while BRCA1-Δ11q+ L304P–expressing cells had undetectable BRCA1 and RAD51 IRIF (Fig. 3E). Immunoprecipitation of ectopic BRCA1 from MDA-MB-436 cells suggested that BRCA1-Δ11q interacted, although less efficiently, with functional protein partners for full-length BRCA1 (Fig. 3F). We also demonstrated ectopic BRCA1-Δ11q provided therapy resistance in HCC1395 cells and in a mouse embryonic stem cell system (Supplementary Fig. S5; ref. 42).

BRCA1-Δ11q promotes resistance *in vivo*

To examine the significance of *BRCA1-Δ11q* expression in tumors, we first measured PARPi responsiveness and *BRCA1* isoform expression in two individual *BRCA1* exon 11–mutant PDX models. Despite both PDX models harboring the same *BRCA1*-exon 11 2080delA mutation (Supplementary Fig. S2), PDX124 tumors were sensitive and PDX196 tumors were resistant to olaparib treatment (Fig. 4A). We confirmed that tumors did not have reversion mutations or gene rearrangements (Supplementary Fig. S2). Similar to exon 11–mutant cell lines, both PDX124 and PDX196 expressed higher levels of Δ11q compared with +11 mRNA, relative to MDA-MB-231 control cells. However, *BRCA1* mRNA levels were significantly greater in PDX196 tumors than in PDX124 tumors, with 26- (P = 0.0001) and 23-fold (P < 0.0001) higher levels of both +11 and Δ11q, respectively (Fig. 4B). BRCA1-Δ11q protein expression was detectable in olaparib-resistant PDX196 tumors, as well as PDX124 tumors that eventually grew through olaparib treatment (Fig. 4C). BRCA1 foci formation was also readily detectable in PDX196 tumors (Fig. 4D).

To further assess the impact of BRCA1-Δ11q on therapy resistance *in vivo*, we utilized the MDA-MB-436 isogenic cell line panel for xenograft experiments. At 30 days post tumor implantation, rucaparib or cisplatin treatment delayed mean tumor growth 6.8- (P < 0.0001) and 12.9-fold (P < 0.0001), respectively, compared with vehicle-treated mice with mCherry-overexpressing MDA-MB-436 tumors. In contrast, rucaparib and cisplatin treatment delayed mean tumor growth 1.1-fold (P = 0.4455) and 1.28-fold (P = 0.2537) in BRCA1 wild-type and 1.4-fold (P = 0.0872) and 2.3-fold (P = 0.019) in BRCA1-Δ11q–overexpressing tumors, respectively, compared with vehicle-treated mice (Fig. 4E and F).

Kaplan–Meier analyses indicated that the median overall survival (OS) of mice harboring mCherry-expressing tumors that were treated with rucaparib or cisplatin increased 1.7-fold (P = 0.0016, log-rank test) and 2-fold (P = 0.0016, log-rank test), respectively, compared with vehicle treated mice. In contrast, in mice harboring BRCA1 wild-type tumors that were treated with rucaparib or cisplatin, median OS increased 1.3-fold (P = 0.0071, log-rank test) and 1.4-fold (P = 0.0048, log-rank test), respectively, and in mice harboring BRCA1-Δ11q tumors treated with rucaparib or cisplatin median OS increased 1.2-fold (P = 0.1536, log-rank test) and 1.5-fold (P = 0.0333, log-rank test), respectively, compared with vehicle-treated mice (Fig. 4G).

Short-term assessment of pharmacodynamics markers showed that rucaparib increased γ-H2AX positivity similarly in all tumors, but wild-type and BRCA1-Δ11q tumors had 4.5- ($P < 0.0001$) and 2.2-fold ($P = 0.005$) lower γ-H2AX positivity, respectively, after cisplatin treatment compared with mCherry-expressing tumors. In addition, wild-type and BRCA1-Δ11q tumors treated with rucaparib had 2.2- ($P = 0.0007$) and 2.5-fold ($P = 0.0059$) higher Ki67 positivity, respectively; and tumors treated with cisplatin had 2.6- ($P < 0.0001$) and 3.7-fold ($P = 0.0003$) higher Ki67 positivity, respectively, compared with mCherry-expressing tumors (**Fig. 4G**). In contrast to *in vitro* data, the degree of PARPi or cisplatin rescue afforded by BRCA1-Δ11q overexpression was more similar to BRCA1 full-length *in vivo*.

Assessment of *BRCA1* exon 11 mutations and patient survival

Because exon 11–mutant tumors were capable of expressing *BRCA1-Δ11q*, we assessed survival outcomes of patients with frameshift mutations located inside (IE11) versus outside (OE11) of exon 11. We analyzed 5-year OS data from the time of initial diagnosis in patients with serous ovarian carcinoma from a previously reported study (**43**). Here, participants with *BRCA1* frameshift mutations OE11 ($n = 231$, 43%; 95% CI, 36%–49%) presented better OS than noncarriers ($n = 1{,}333$, 33%; 95% CI, 30%–36%; $P = 0.002$, log-rank test) as well as participants with frameshift mutations IE11 ($n = 148$, 31%; 95% CI, 23%–39%; $P = 0.02$, log-rank test) at 5 years of follow up. Moreover, participants with frameshift mutations IE11 presented with 5-year OS similar to noncarriers ($P = 0.84$, log-rank test; **Fig. 5A**, Supplementary Tables S3 and S4).

Although patients with exon 11 mutations demonstrated worse 5-year survival, we hypothesized that, similar to our PDX data, *BRCA1-Δ11q* might only be highly expressed in a fraction of exon 11–mutant tumors, and so not all exon 11–mutant patients would necessarily be resistant to therapy. Analyses of primary tumors (unrelated to the above studies) with mutations IE11 showed variable levels of *BRCA1-Δ11q* expression. Tumor #317 expressed 2.7- ($P = 0.0227$) and 4-fold ($P = 0.0117$) greater levels of Δ11q compared with tumor #325 and tumor #411, respectively, despite all tumors harboring deleterious exon 11 mutations (**Fig. 5B**).

Inhibition of splicing increases PARPi sensitivity

Because high levels of BRCA1-Δ11q expression were required for residual function, we hypothesized that limiting splicing-dependent excision of exon 11q might provide an opportunity to enhance PARPi sensitivity. We first identified two binding elements for the FOX2 splicing site selection factor at position +18 and +63 downstream from the cryptic splice site location (Supplementary Fig. S6; refs. **44, 45**). Depletion of FOX2 using 2 individual siRNAs did not impact +11 expression levels, but reduced Δ11q expression 1.7- ($P = 0.0043$) and 1.6-fold ($P = 0.0179$) in MDA-MB-231, 1.5- ($P = 0.048$) and 1.6-fold ($P = 0.0301$) in UWB1.289, 2.2- ($P = 0.0056$) and 3.1-fold ($P = 0.0017$) in SUM149PT cells, compared with scrambled siRNA–treated cells, respectively (**Fig. 6A**). At the protein level, densitometric analyses of Western blots indicated FOX2 siRNA did not impact full-length BRCA1 protein expression, but BRCA1-Δ11q levels were reduced 2.9- and 2.2-fold in MDA-MB-231, 2- and 2.8-fold in UWB1.289, 1.9- and 1.8-fold in SUM149PT cells, compared with scrambled siRNA–treated cells (**Fig. 6B**). FOX2 siRNA had no impact on MDA-MB-231 cells PARPi sensitivity, but reduced the LC_{50} value of rucaparib 3.8- ($P = 0.0063$) and 27.4-fold ($P = 0.0017$) in UWB1.289 cells, as well as 1.9- ($P = 0.0237$) and 5-fold ($P = 0.0002$) in SUM149PT cells, compared with scrambled siRNA–treated cells (**Fig. 6C**). Furthermore, BRCA1-minigene analyses demonstrated that mutation of FOX2-binding motifs also partially decreased Δ11q-reporter mRNA and protein levels (**Fig. 6D**).

We next investigated the ability of PI-B, a small-molecule inhibitor of the U2 snRNP spliceosome machinery (**46**), to disrupt *BRCA1-Δ11q* production. PI-B treatment reduced both +11 and Δ11q mRNA expression; however, the relative reduction in Δ11q levels was 7.7- ($P = 0.002$) and 7-fold ($P = 0.016$) greater compared with the reduction in +11 levels in MDA-MB-231 and UWB1.289 cells, respectively (**Fig. 6E**). Furthermore, full-length BRCA1 protein levels were reduced but

remained readily detectable after treatment with up to 10 nmol/L PI-B in MDA-MB-231 cells. However, BRCA1-Δ11q protein levels were barely detectable at 1.25 nmol/L PI-B in both MDA-MB-231 and UWB1.289 cells (Fig. 6F). Simultaneous incubation with both PI-B and rucaparib did not significantly impact MDA-MB-231 cells, but resulted in a 2.8- (P = 0.0296) and 2.1-fold (P = 0.0426) reduction in colony formation compared with cells treated with rucaparib only in UWB1.289 and SUM149PT cells, respectively (Fig. 6G). Furthermore, ectopic overexpression of a BRCA1-Δ11q cDNA that did not depend on exon 11q splicing, resulted in a 1.9-fold (P = 0.001) rescue in colony formation in cells treated with the PI-B and rucaparib combination, compared with GFP-expressing control cells (Fig. 6H), suggesting that PI-B–induced PARPi sensitization was mediated, in part, through the reduction in BRCA1-Δ11q levels.

Discussion

In the current study, we provide evidence that *BRCA1* splice isoforms lacking exon 11 are capable of producing truncated but hypomorphic proteins. It was previously shown that the exon 11–deficient Brca1-Δ11 isoform partially compensates for the lack of other Brca1 isoforms during embryogenesis (31–33, 47). Here, we show that BRCA1-Δ11q can also partially compensate for full-length BRCA1 in response to homologous recombination targeting therapeutics. BRCA1-Δ11q retains, although less efficiently, many of the protein–protein interactions carried out by full-length BRCA1. We identified the BRCA1–Δ11q–PALB2 interaction as critical for BRCA1-Δ11q–mediated RAD51 IRIF and resistance.

BRCA1-Δ11q was expressed in *BRCA1* wild-type as well as exon 11–mutant cell lines. Although frameshift mutations in exon 11 resulted in the NMD of exon 11 containing transcripts, they did not impact the rate of alternative splicing or directly affect *BRCA1-Δ11q* levels. In support of this, PDX124 and PDX196 tumors both harbored identical 2080delA exon 11 mutations; however, both +11 and Δ11q transcript levels were significantly higher in PDX196 relative to PDX124 tumors, suggesting that overall *BRCA1* gene transcription, rather than the rate of alternative exon splicing, was elevated. Both patients whose tumors were used to derive PDX124 and PDX196 initially demonstrated clinical responsiveness to olaparib therapy; while PDX124 was derived prior to the patient starting olaparib therapy, PDX196 was derived at the time of clinical tumor progression on olaparib. We anticipate that high levels of *BRCA1-Δ11q* expression may be selected for in response to chemotherapy. Primary patient tumors harboring exon 11 mutations also demonstrated variable *BRCA1-Δ11q* levels, and this isoform might only be overexpressed in a subset of exon 11 mutation carriers. Additional resistance mechanisms such as secondary reversion mutations have also been shown to occur in tumors with exon 11 mutations (48, 49).

Intriguingly, our analyses indicated that exon 11 mutation carriers with ovarian cancer had a worse 5-year overall survival compared with non-exon 11 mutation carriers (Fig. 5A). Another recent study of mutation-specific cancer risks identified the exon 11 region of *BRCA1* as an ovarian cancer cluster region, where mutation carriers had a relative decrease in breast relative to ovarian cancer risk (50). Further work is required to determine whether BRCA1-Δ11q has any impact on long-term survival outcomes or breast versus ovarian tissue–specific phenotypes.

Currently, an understanding of PARPi and platinum resistance is incomplete. Our findings provide evidence for a role of the BRCA1-Δ11q alternative splice isoform in promoting resistance. Moreover, we show that inhibition of the spliceosome reduced BRCA1-Δ11q levels and sensitized exon 11–mutant cell lines to PARPi, potentially offering a strategy to resensitize tumors that express high levels of BRCA1-Δ11q.

References

1. Szabo CI, King MC. Inherited breast and ovarian cancer. Hum Mol Genet 1995;4:1811–7.

2. Friedman LS, Ostermeyer EA, Szabo CI, Dowd P, Lynch ED, Rowell SE, et al. Confirmation of BRCA1 by analysis of germline mutations linked to breast and ovarian cancer in ten families. Nat Genet 1994;8:399–404.

3. Perrin-Vidoz L, Sinilnikova OM, Stoppa-Lyonnet D, Lenoir GM, Mazoyer S. The nonsense-mediated mRNA decay pathway triggers degradation of most BRCA1 mRNAs bearing premature termination codons. Hum Mol Genet 2002;11:2805–14.

4. Moynahan ME, Cui TY, Jasin M. Homology-directed dna repair, mitomycin-c resistance, and chromosome stability is restored with correction of a Brca1 mutation. Cancer Res 2001;61:4842–50.

5. Scully R, Chen J, Ochs RL, Keegan K, Hoekstra M, Feunteun J, et al. Dynamic changes of BRCA1 subnuclear location and phosphorylation state are initiated by DNA damage. Cell 1997;90:425–35.

6. Lord CJ, Tutt AN, Ashworth A. Synthetic lethality and cancer therapy: lessons learned from the development of PARP inhibitors. Annu Rev Med 2015;66:455–70.

7. Lord CJ, Ashworth A. Mechanisms of resistance to therapies targeting BRCA-mutant cancers. Nat Med 2013;19:1381–8.

8. Bryant HE, Schultz N, Thomas HD, Parker KM, Flower D, Lopez E, et al. Specific killing of BRCA2-deficient tumours with inhibitors of poly(ADP-ribose) polymerase. Nature 2005;434:913–7.

9. Farmer H, McCabe N, Lord CJ, Tutt AN, Johnson DA, Richardson TB, et al. Targeting the DNA repair defect in BRCA mutant cells as a therapeutic strategy. Nature 2005;434:917–21.

10. Kennedy RD, Quinn JE, Mullan PB, Johnston PG, Harkin DP. The role of BRCA1 in the cellular response to chemotherapy. J Natl Cancer Inst 2004;96:1659–68.

11. Quinn JE, Kennedy RD, Mullan PB, Gilmore PM, Carty M, Johnston PG, et al. BRCA1 functions as a differential modulator of chemotherapy-induced apoptosis. Cancer Res 2003;63:6221–8.

12. Gelmon KA, Tischkowitz M, Mackay H, Swenerton K, Robidoux A, Tonkin K, et al. Olaparib in patients with recurrent high-grade serous or poorly differentiated ovarian carcinoma or triple-negative breast cancer: a phase 2, multicentre, open-label, non-randomised study. Lancet Oncol 2011;12:852–61.

13. Sandhu SK, Schelman WR, Wilding G, Moreno V, Baird RD, Miranda S, et al. The poly(ADP-ribose) polymerase inhibitor niraparib (MK4827) in BRCA mutation carriers and patients with sporadic cancer: a phase 1 dose-escalation trial. Lancet Oncol 2013;14:882–92.

14. Ang JE, Gourley C, Powell B, High H, Shapira-Frommer R, Castonguay V, et al. Efficacy of chemotherapy in BRCA1/2 mutation carrier ovarian cancer in the setting of poly(ADP-ribose) polymerase inhibitor resistance: a multi-institutional study. Clin Cancer Res 2013;19:5485–93.

15. Ledermann J, Harter P, Gourley C, Friedlander M, Vergote I, Rustin G, et al. Olaparib maintenance therapy in patients with platinum-sensitive relapsed serous ovarian cancer: a

preplanned retrospective analysis of outcomes by BRCA status in a randomised phase 2 trial. Lancet Oncol 2014;15:852–61.

16. Edwards SL, Brough R, Lord CJ, Natrajan R, Vatcheva R, Levine DA, et al. Resistance to therapy caused by intragenic deletion in BRCA2. Nature 2008;451:1111–5.

17. Sakai W, Swisher EM, Karlan BY, Agarwal MK, Higgins J, Friedman C, et al. Secondary mutations as a mechanism of cisplatin resistance in BRCA2-mutated cancers. Nature 2008;451:1116–20.

18. Bouwman P, Aly A, Escandell JM, Pieterse M, Bartkova J, van der Gulden H, et al. 53BP1 loss rescues BRCA1 deficiency and is associated with triple-negative and BRCA-mutated breast cancers. Nat Struct Mol Biol 2010;17:688–95.

19. Bunting SF, Callen E, Wong N, Chen HT, Polato F, Gunn A, et al. 53BP1 inhibits homologous recombination in Brca1-deficient cells by blocking resection of DNA breaks. Cell 2010;141:243–54.

20. Johnson N, Johnson SF, Yao W, Li YC, Choi YE, Bernhardy AJ, et al. Stabilization of mutant BRCA1 protein confers PARP inhibitor and platinum resistance. Proc Natl Acad Sci U S A 2013;110:17041–6.

21. Drost R, Bouwman P, Rottenberg S, Boon U, Schut E, Klarenbeek S, et al. BRCA1 RING function is essential for tumor suppression but dispensable for therapy resistance. Cancer Cell 2011;20:797–809.

22. Rottenberg S, Jaspers JE, Kersbergen A, van der Burg E, Nygren AO, Zander SA, et al. High sensitivity of BRCA1-deficient mammary tumors to the PARP inhibitor AZD2281 alone and in combination with platinum drugs. Proc Natl Acad Sci U S A 2008;105:17079–84.

23. Colombo M, Blok MJ, Whiley P, Santamarina M, Gutierrez-Enriquez S, Romero A, et al. Comprehensive annotation of splice junctions supports pervasive alternative splicing at the BRCA1 locus: a report from the ENIGMA consortium. Hum Mol Genet 2014;23:3666–80.

24. Thomassen M, Blanco A, Montagna M, Hansen TV, Pedersen IS, Gutierrez-Enriquez S, et al. Characterization of BRCA1 and BRCA2 splicing variants: a collaborative report by ENIGMA consortium members. Breast Cancer Res Treat 2012;132:1009–23.

25. Romero A, Garcia-Garcia F, Lopez-Perolio I, Ruiz de Garibay G, Garcia-Saenz JA, Garre P, et al. BRCA1 Alternative splicing landscape in breast tissue samples. BMC Cancer 2015;15:219.

26. Orban TI, Olah E. Expression profiles of BRCA1 splice variants in asynchronous and in G1/S synchronized tumor cell lines. Biochem Biophys Res Commun 2001;280:32–8.

27. Tammaro C, Raponi M, Wilson DI, Baralle D. BRCA1 exon 11 alternative splicing, multiple functions and the association with cancer. Biochem Soc Trans 2012;40:768–72.

28. Raponi M, Smith LD, Silipo M, Stuani C, Buratti E, Baralle D. BRCA1 exon 11 a model of long exon splicing regulation. RNA Biol 2014;11:351–9.

29. Orban TI, Olah E. Emerging roles of BRCA1 alternative splicing. Mol Pathol 2003;56:191–7.

30. Wilson CA, Payton MN, Elliott GS, Buaas FW, Cajulis EE, Grosshans D, et al. Differential subcellular localization, expression and biological toxicity of BRCA1 and the splice variant BRCA1-delta11b. Oncogene 1997;14:1–16.

31. Ludwig T, Chapman DL, Papaioannou VE, Efstratiadis A. Targeted mutations of breast cancer susceptibility gene homologs in mice: lethal phenotypes of Brca1, Brca2, Brca1/Brca2, Brca1/p53, and Brca2/p53 nullizygous embryos. Genes Dev 1997;11:1226–41.

32. Xu X, Qiao W, Linke SP, Cao L, Li WM, Furth PA, et al. Genetic interactions between tumor suppressors Brca1 and p53 in apoptosis, cell cycle and tumorigenesis. Nat Genet 2001;28:266–71.

33. Xu X, Wagner KU, Larson D, Weaver Z, Li C, Ried T, et al. Conditional mutation of Brca1 in mammary epithelial cells results in blunted ductal morphogenesis and tumour formation. Nat Genet 1999;22:37–43.

34. NIH National Human Genome Research Institute. Breast Cancer Information Core. Available from: https://research.nhgri.nih.gov/projects/bic/index.shtml.

35. Thompson D, Easton D, Breast Cancer Linkage C. Variation in BRCA1 cancer risks by mutation position. Cancer Epidemiol Biomarkers Prev 2002;11:329–36.

36. Risch HA, McLaughlin JR, Cole DE, Rosen B, Bradley L, Fan I, et al. Population BRCA1 and BRCA2 mutation frequencies and cancer penetrances: a kin-cohort study in Ontario, Canada. J Natl Cancer Inst 2006;98:1694–706.

37. Risch HA, McLaughlin JR, Cole DE, Rosen B, Bradley L, Kwan E, et al. Prevalence and penetrance of germline BRCA1 and BRCA2 mutations in a population series of 649 women with ovarian cancer. Am J Hum Genet 2001;68:700–10.

38. Barbier J, Dutertre M, Bittencourt D, Sanchez G, Gratadou L, de la Grange P, et al. Regulation of H-ras splice variant expression by cross talk between the p53 and nonsense-mediated mRNA decay pathways. Mol Cell Biol 2007;27:7315–33.

39. Williams RS, Chasman DI, Hau DD, Hui B, Lau AY, Glover JN. Detection of protein folding defects caused by BRCA1-BRCT truncation and missense mutations. J Biol Chem 2003;278:53007–16.

40. Williams RS, Glover JN. Structural consequences of a cancer-causing BRCA1-BRCT missense mutation. J Biol Chem 2003;278:2630–5.

41. Sy SM, Huen MS, Chen J. PALB2 is an integral component of the BRCA complex required for homologous recombination repair. Proc Natl Acad Sci U S A 2009;106:7155–60.

42. Bouwman P, van der Gulden H, van der Heijden I, Drost R, Klijn CN, Prasetyanti P, et al. A high-throughput functional complementation assay for classification of BRCA1 missense variants. Cancer Discov 2013;3:1142–55.

43. Bolton KL, Chenevix-Trench G, Goh C, Sadetzki S, Ramus SJ, Karlan BY, et al. Association between BRCA1 and BRCA2 mutations and survival in women with invasive epithelial ovarian cancer. JAMA 2012;307:382–90.

44. Venables JP, Klinck R, Koh C, Gervais-Bird J, Bramard A, Inkel L, et al. Cancer-associated regulation of alternative splicing. Nat Struct Mol Biol 2009;16:670–6.

45. Huang SC, Ou AC, Park J, Yu F, Yu B, Lee A, et al. RBFOX2 promotes protein 4.1R exon 16 selection via U1 snRNP recruitment. Mol Cell Biol 2012;32:513–26.

46. Kotake Y, Sagane K, Owa T, Mimori-Kiyosue Y, Shimizu H, Uesugi M, et al. Splicing factor SF3b as a target of the antitumor natural product pladienolide. Nat Chem Biol 2007;3:570–5.

47. Huber LJ, Yang TW, Sarkisian CJ, Master SR, Deng CX, Chodosh LA. Impaired DNA damage response in cells expressing an exon 11-deleted murine Brca1 variant that localizes to nuclear foci. Mol Cell Biol 2001;21:4005–15.

48. Norquist B, Wurz KA, Pennil CC, Garcia R, Gross J, Sakai W, et al. Secondary somatic mutations restoring BRCA1/2 predict chemotherapy resistance in hereditary ovarian carcinomas. J Clin Oncol 2011;29:3008–15.

49. Patch AM, Christie EL, Etemadmoghadam D, Garsed DW, George J, Fereday S, et al. Whole-genome characterization of chemoresistant ovarian cancer. Nature 2015;521:489–94.

50. Rebbeck TR, Mitra N, Wan F, Sinilnikova OM, Healey S, McGuffog L, et al. Association of type and location of BRCA1 and BRCA2 mutations with risk of breast and ovarian cancer. JAMA 2015;313:1347–61.

Figure 1.*BRCA1* exon 11–mutant cell lines express BRCA1-Δ11q.
A, cell lines were analyzed for BRCA1 and tubulin levels by Western blot analysis. *, predicted BRCA1 locations, molecular weights are indicated. B, cells were treated with scrambled (Sc) or BRCA1-Δ11q (11q) siRNA and analyzed by Western blot analysis. C, exon 11 containing (+11) *BRCA1* transcripts and the *BRCA1-Δ11q* (Δ11q) isoform were detected using qRT-PCR. Values were normalized to a HKG, expressed as a percentage of MDA-MB-231 cells. D, 293T cells were transfected with either GFP-control or BRCA1-minigene reporter constructs that were wild-type (WT) or carrying mutations that disrupted the cryptic 11q splice site (11q), or with frameshift mutations (M1:2288delT; M2:2529C>T; M3:3960C>T). BRCA1-Δ11q-reporter mRNA and protein expression was measured by RT-PCR (top) and Western blot analysis (bottom); see Supplementary Fig. S3. E, CRISPR/Cas9 targeting the mutation-containing region of exon 11 (sg_exon11)-generated SUM149PT clones (C) 1–4; see Supplementary Fig. S4. +11 and Δ11q mRNA was measured using qRT-PCR (left); values were normalized to a HKG and expressed as a percentage of sg_GFP control cells. BRCA1 protein was detected by Western blot analysis (right). F, the indicated cell lines were treated with vehicle or 10 μg/mL CHX for 5 hours, followed by assessment of +11 (left) and Δ11q (right) levels by qRT-PCR. G, cells were treated with either vehicle (V), 10 μg/mL CHX (C), 5 μg/mL ACT (A), or A and C simultaneously for 5 hours and assessed for +11 expression by qRT-PCR. H, cells were treated with either vehicle (V) or 5 μg/mL ACT (A) for 5 hours and assessed for Δ11q expression by qRT-PCR. *, $P < 0.05$.

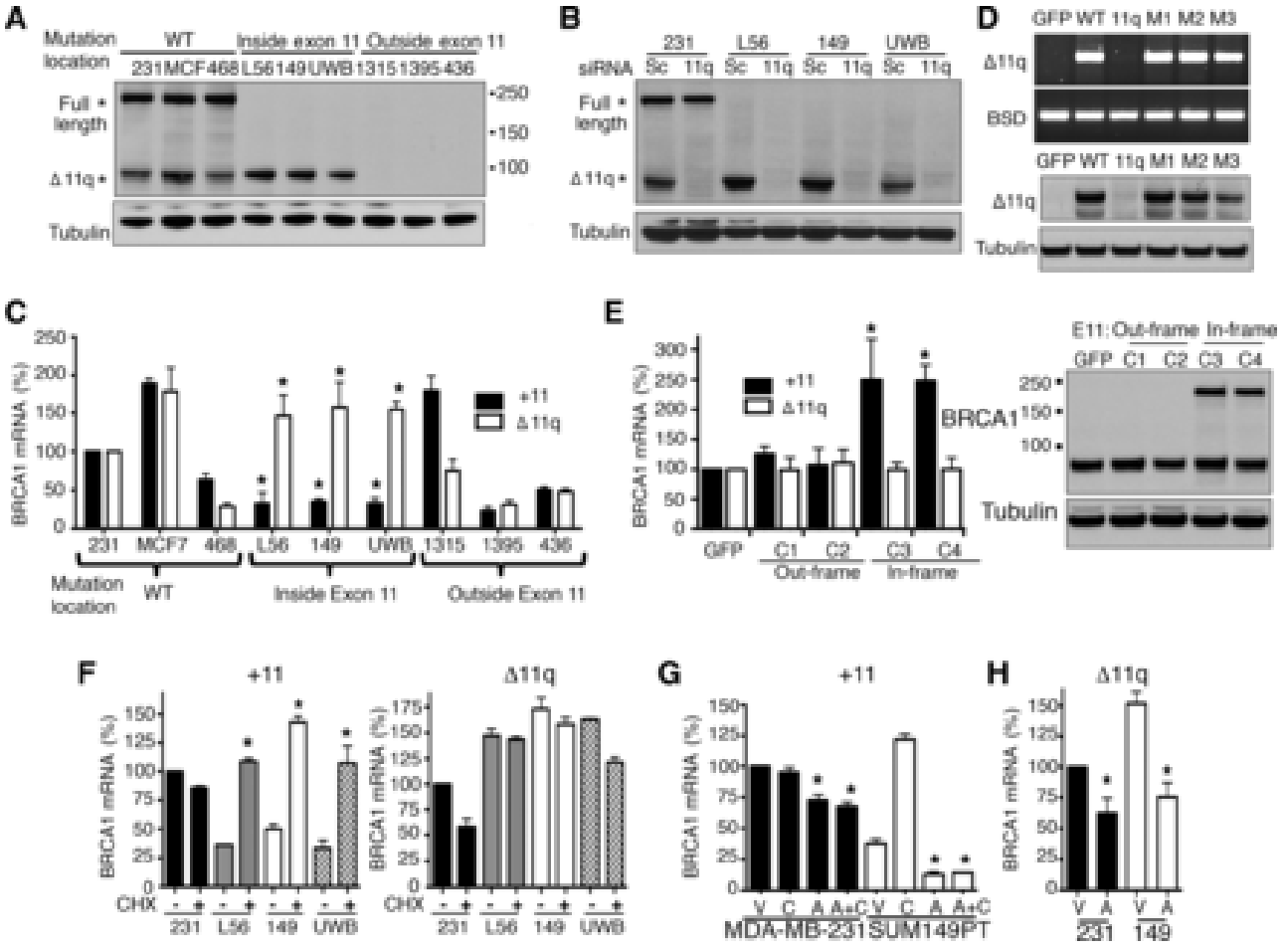

Figure 2. Exon 11–mutant cells are less sensitive to PARPi and cisplatin treatment.
A, cells were untreated (no Rx) or treated with IR (10 Gy) and subject to immunofluorescence to detect BRCA1, RAD51, and γ-H2AX foci; representative images of IR-treated cells. Mean ± SEM foci-positive cells are expressed as a percentage of total geminin-positive cells. B, cell lines were treated with rucaparib, olaparib, cisplatin, or taxol and colony formation assessed; graphs represent three independent experiments, mean ± SEM LC_{50} values; see Supplementary Table S2 for fold changes and P values. C, cells were maintained in the presence of vehicle, 100 nmol/L rucaparib (left), or 20 ng/mL cisplatin (right) and counted every 4 days. Cell line growth was expressed as a percentage of vehicle-treated cell numbers counted on the same day. Mean ± SEM from three technical replicates. D, UWB1.289 vehicle-, rucaparib (R)-, and cisplatin (C)-treated cell lysates were collected at days 25 and 50 for Western blot analysis. E, assessment of BRCA1, RAD51, and γ-H2AX foci by immunofluorescence as for A. Western blot analysis (top) shows BRCA1-Δ11q was depleted using two individual BRCA1 targeting shRNAs. Representative images (bottom) of IR-treated cells and mean ± SEM foci-positive cells are expressed as a percentage of total geminin-positive cells (right). F, cells described in E were treated with rucaparib or cisplatin and colony formation assessed; three independent experiments, mean ± SEM; LC_{50} concentrations are shown; see Supplementary Table S2. *, $P < 0.05$.

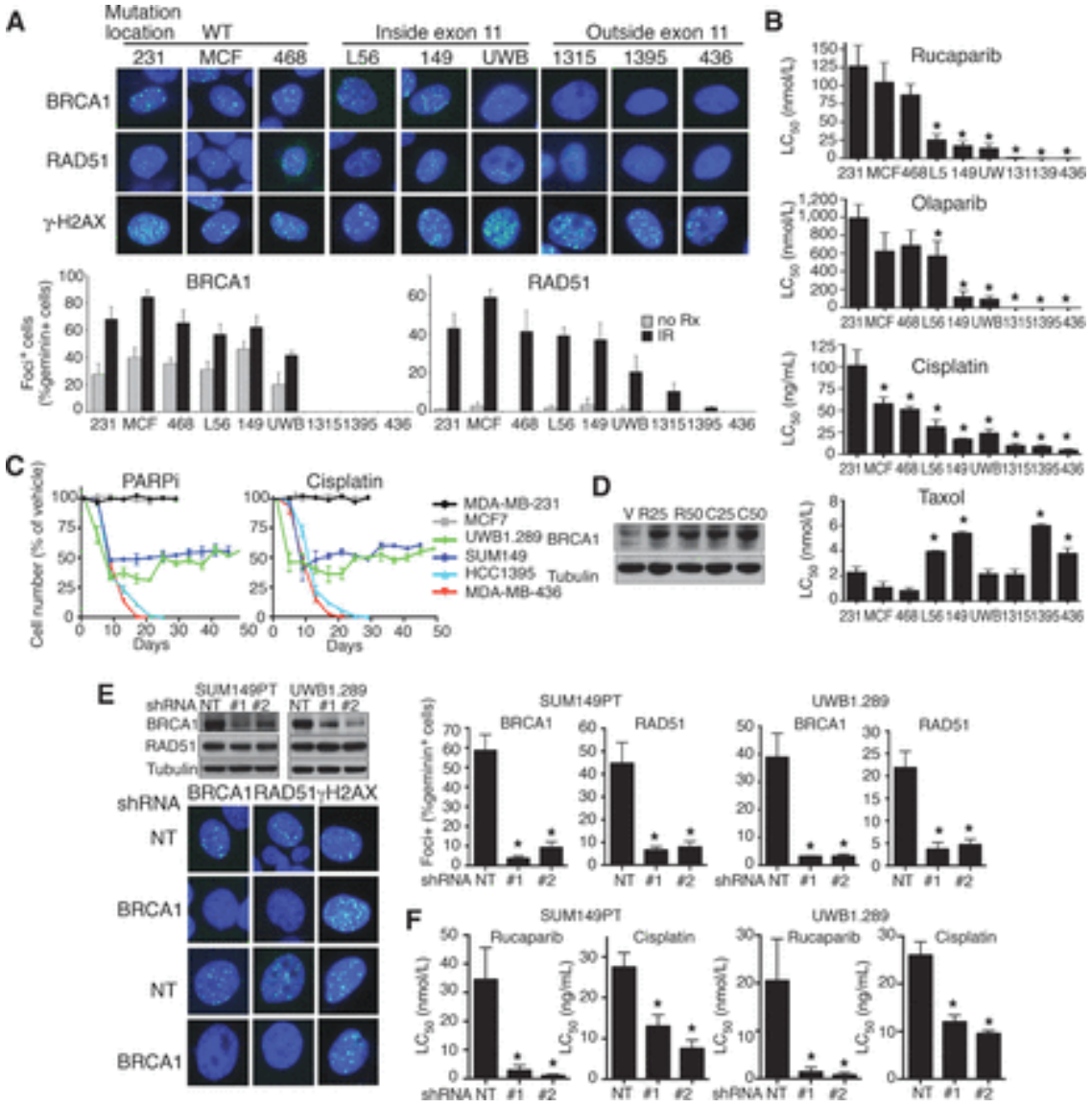

Figure 3. BRCA1-Δ11q provides partial resistance to therapy *in vitro*.
A, CRISPR/Cas9 gene targeting the SUM149PT *BRCA1* mutation-containing region of exon 11 (sg_exon11) did not affect the reading frame (OF) in clones 1, 2, or restored the reading frame (IF) in clones 3, 4. Targeting of exon 22 (sg_exon22) resulted in frameshift mutations and loss of BRCA1 expression. Cells treated with sg_GFP were used as a control. BRCA1 protein was detected by Western blot analysis. See Supplementary Fig. S4 for more details. B, cells described in A were treated with rucaparib or cisplatin and colony formation assessed. C, MDA-MB-436 cells expressing mCherry, BRCA1 full-length, BRCA1-Δ11q, or BRCA1-Δ11q+L304P were assessed for BRCA1 protein expression by Western blot analysis. D, cells described in C were treated with rucaparib or cisplatin and colony formation assessed. E, cells described in C were treated with IR (10 Gy) and subject to immunofluorescence to detect BRCA1, RAD51, and γ-H2AX foci, as well as geminin and DAPI staining; representative images of IR-treated cells. Double geminin and BRCA1- or RAD51-positive cells were counted and expressed as a percentage of total geminin-positive cells; bars show mean ± SEM of geminin+BRCA1 or RAD51 foci-positive cells from three independent experiments. F, cells described in C were subject to immunoprecipitation using an anti-HA antibody and Western blotting with the indicated antibodies. *, $P < 0.05$.

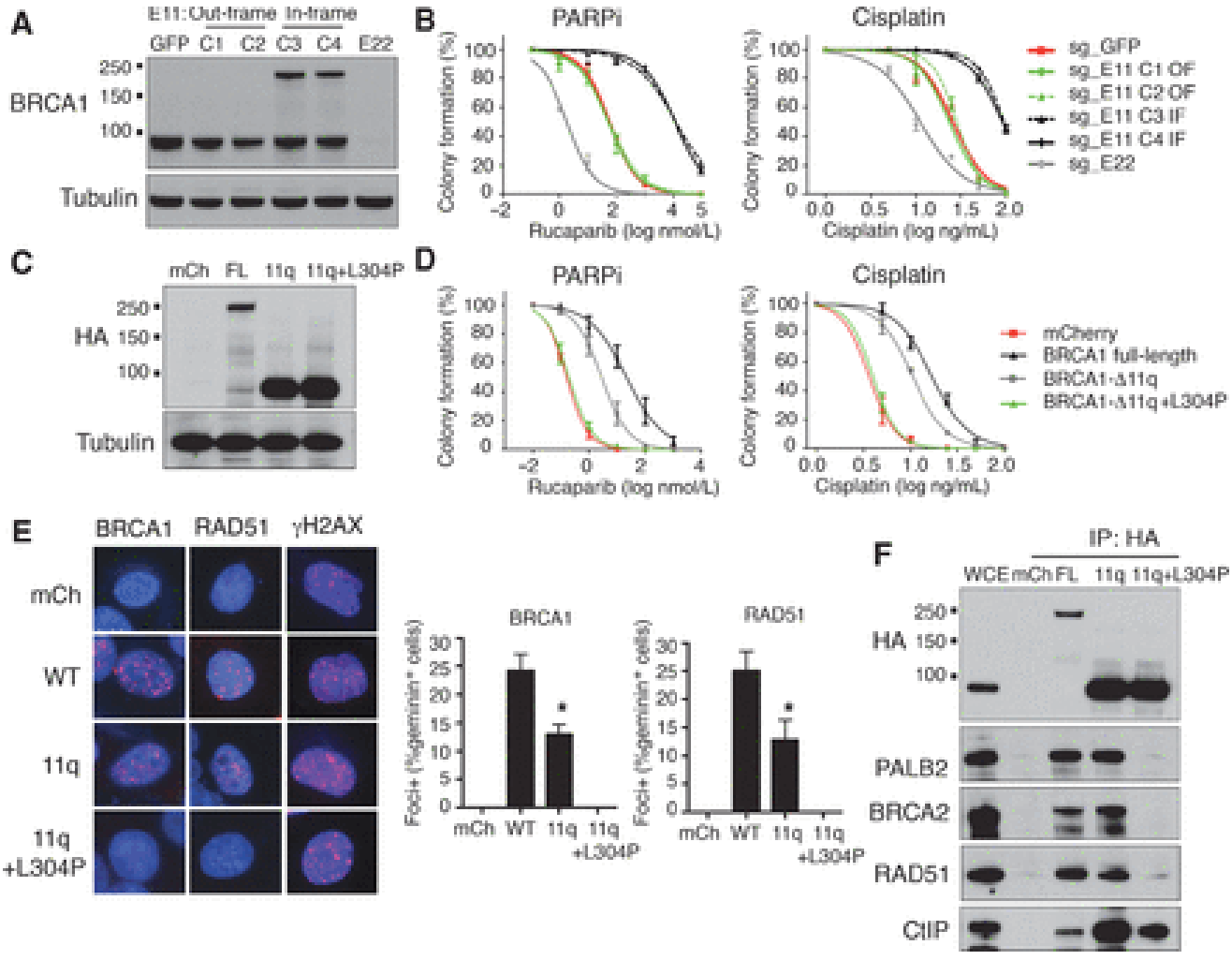

Figure 4. BRCA1-Δ11q promotes resistance *in vivo*.
A, PDX124 ($n \geq 8$ mice; left) and PDX196 ($n \geq 3$ mice; right) tumors were treated with vehicle (black lines) or olaparib (green lines) and tumor volume measured. B, PDX tumors were harvested from three individual untreated mice and assessed for +11 and Δ11q expression by qRT-PCR. Values were normalized to the *POL2RF* HKG control and expressed as a percentage of the values calculated for MDA-MB-231 cells. C, MDA-MB-231 cells were prepared for whole cell extract (WCE) as well as tumor xenografts and used as positive controls, and compared with PDX127 (*BRCA1*^{185delAG}-mutant control, $n = 1$), PDX196 ($n = 2$), PDX124 OS (growth inhibition with olaparib, $n = 1$), and OR (growth slowed with olaparib, $n = 2$) tumors for Western blotting. D, mice harboring PDX196 tumors were treated with vehicle or olaparib and tumors assessed for BRCA1 foci formation as well as geminin staining; representative images (left) and quantification of BRCA1 mean ± SEM foci geminin-positive cells. E, MDA-MB-436 tumor xenografts expressing mCherry, BRCA1 wild-type, and BRCA1-Δ11q were treated with vehicle (black lines), rucaparib (green lines), or cisplatin (red lines) and tumor growth measured; lines represent individual tumors and mice ($n = 5$). F, individual tumor volumes at day 30 are shown. G, Kaplan–Meier survival analyses for mice described in E. H, Mice were treated as in E for 4 days, tumors were assessed for γ-H2AX and Ki67 staining by IHC. Representative images, scale bars, 50 μm. Mean ± SEM quantification of staining intensities. *, $P < 0.05$.

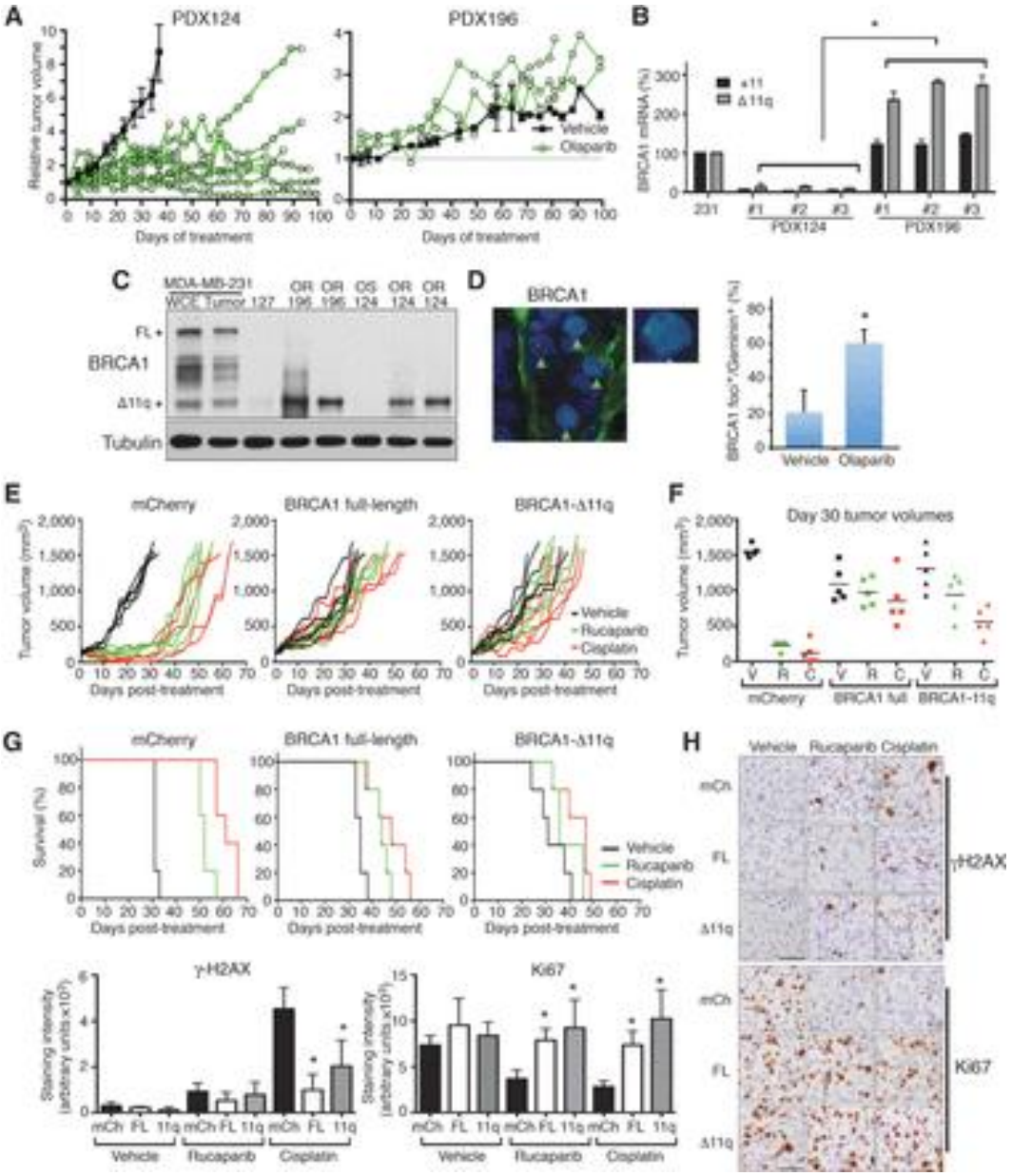

Figure 5. BRCA1 exon 11 mutations and patient survival.
A, Kaplan–Meier estimates of cumulative survival according to *BRCA1* mutation group of serous ovarian cancer patients (see Supplementary Tables S3 and S4). B, primary breast and ovarian cancer patient tumors (unrelated to studies described in A) were subject to qRT-PCR analysis for +11 and Δ11q expression. Values were normalized to a HKG control and expressed as a percentage of the values calculated for MDA-MB-231 cells. *, $P < 0.05$.

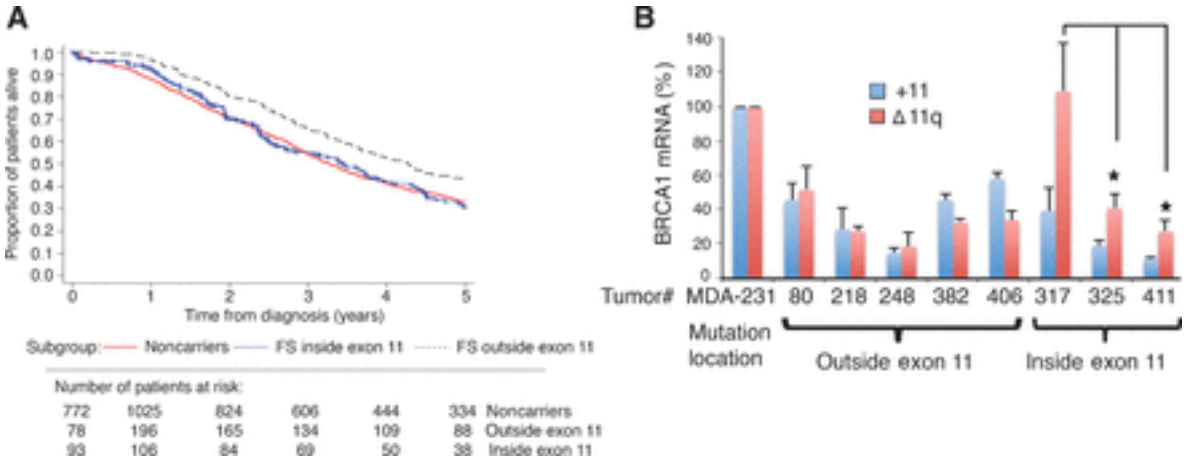

Figure 6. Splicing inhibition sensitizes exon 11–mutant cells to PARPi.
A, MDA-MB-231, UWB1.289, and SUM149PT cells were transfected with scrambled (Sc) or FOX2#1 and FOX2#2 siRNA and *FOX2*, *POLR2F*, +11 and Δ11q *BRCA1* isoform mRNA levels measured by qRT-PCR. Values were normalized to *POLR2F* HKG expression and expressed as a percentage of MDA-MB-231 cells. B, cells treated as in A were subject to Western blotting. C, cells treated as in A were subject to 3-day rucaparib and cisplatin exposure and reseeded for colony formation. Mean ± SEM. LC_{50}values are shown. D, 293T cells were transfected with BRCA1 minigene reporter constructs as in **Fig. 1D** and Supplementary Fig. S3, with FOX2-binding sites mutated (FOX). BRCA1-Δ11q-reporter construct mRNA and protein expression was measured by RT-PCR (left) and Western blot analysis (right), respectively. E, MDA-MB-231 and UWB1.289 cells incubated with PI-B (10 nmol/L) and mRNA levels measured by qRT-PCR. Values were expressed as a percentage of vehicle-treated MDA-MB-231 cells or UWB1.289 cells. F, cells were treated with increasing concentrations of PI-B and subject to Western blotting. G, cells were treated with vehicle (−) or PI-B (+; 1.25 nmol/L) and either vehicle or rucaparib (100 nmol/L) for 72 hours and reseeded for colony formation assay; mean ± SEM colony formation of rucaparib-treated cells calculated as a percentage of vehicle-treated cells. H, SUM149PT cells engineered to ectopically express GFP or BRCA1-Δ11q were treated as in G and assessed for colony formation. Western blot analysis (left) and mean ± SEM colony formation of rucaparib-treated cells, calculated as a percentage of vehicle-treated cells (right). *, $P < 0.05$.